*electrochem*

MDPI

*Article*

# Ageing and Water Detection in Hydroscopic Organic Electrolytes

**Eva Alonso-Muñoz [1], Janwa El Maiss [1], Wejdene Gongi [2], Divya Balakrishnan [1], Delphine Faye [3], Karine Mougin [2] and César Pascual García [1,*]**

[1] Luxembourg Institute of Science and Technology, 28 Avenue des Hauts Fourneaux, L-4362 Esch-sur-Alzette, Luxembourg; divya.balakrishnan@list.lu (D.B.)
[2] Institut de Science des Matériaux de Mulhouse (IS2M), 15 rue Jean Starcky, 68057 Mulhouse, France; karine.mougin@uha.fr (K.M.)
[3] Centre National d'Études Spatiales (CNES), 18 Av. Edouard Belin, 31400 Toulouse, France; delphine.faye@cnes.fr
* Correspondence: cesar.pascual@list.lu

**Abstract**

Electrolyte degradation and trace water contamination critically affect the lifetime and safety of lithium-ion batteries. In organic-based electrolytes such as acetonitrile (MeCN), even small amounts of water can trigger $PF_6^-$ hydrolysis, producing HF, $POF_3$, and related species that contribute to electrolyte ageing and alter interfacial reactions. This study explores the electrochemical signatures of ageing and moisture contamination in $Bu_4NPF_6$- and $LiPF_6$-based MeCN electrolytes through a systematic cyclic voltammetry protocol. Platinum electrodes with different surface morphologies—flat, Nafion-coated, and nanostructured—were compared to assess their sensitivity to water-induced degradation. Cathodic Faradaic currents appearing around −0.7 to −1.0 V vs. Ag/AgCl were attributed to the protonic species generated by $PF_6^-$-induced hydrolysis. The presence of $LiPF_6$, commonly used in battery electrolytes, further increases the concentration of anions responsible for the protonic species, therefore contributing to the acceleration of the electrolyte degradation. Experiments using a Nafion proton-conductive membrane assess the protonic origin of these peaks. Meanwhile, nanostructured platinum exhibits approximately four times higher current responses and enhanced sensitivity to water additions, reflecting the influence of surface roughness and active area. Overall, the findings indicate that electrode morphology significantly influences the detectability of ageing- and water-driven reactions, supporting the potential of nanostructured Pt as a diagnostic material for in situ monitoring.

**Keywords:** lithium-ion batteries; electrolyte ageing; water detection; acetonitrile (MeCN); $LiPF_6$ hydrolysis; cyclic voltammetry (CV); hydrogen evolution reaction (HER); platinum electrodes; Nafion coating; nanostructured surfaces

Check for updates

Academic Editor: Masato Sone

Received: 28 November 2025
Revised: 8 January 2026
Accepted: 12 January 2026
Published: 16 January 2026

**Copyright:** © 2026 by the authors. Licensee MDPI, Basel, Switzerland. This article is an open access article distributed under the terms and conditions of the Creative Commons Attribution (CC BY) license.

## 1. Introduction

Electrolyte composition critically affects the lifetime, performance, and safety of lithium-ion batteries [1–3]. Even trace amounts of water can alter electrochemical behaviour by accelerating electrolyte decomposition, promoting solid electrolyte interphase (SEI) formation, and destabilizing electrodes [4–6]. Detecting moisture in aprotic organic-based electrolytes such as acetonitrile (MeCN), which cannot donate protons, remains technically challenging for real-time monitoring during battery operation or research [7]. MeCN was used as a model aprotic solvent due to its wide electrochemical window and well-defined

behaviour on Pt electrodes, enabling clear isolation of protonic species generated by $PF_6^-$ hydrolysis. This simplified environment facilitates mechanistic analysis of water-induced degradation processes. While MeCN is not a practical battery solvent, the identified cathodic signatures are expected to remain relevant in other aprotic electrolytes, with possible shifts in potential arising from solvent-dependent interfacial effects. Over time, solvent molecules react with residual water, trace acids, or salt-derived impurities to form HF, $POF_3$, fluorophosphates, and other products that alter interfacial chemistry and reduce ionic mobility [8,9]. Understanding the mechanisms of solvent degradation—particularly how trace water and salt hydrolysis products drive changes in MeCN-based systems—is therefore important not only for improving the long-term stability and safety of lithium-ion electrolytes in these solvents, but also for advancing the broader use of MeCN–salt combinations in electrochemical and synthetic applications [10]. Industry and best-practice studies typically control electrolyte water to $\leq$10–20 ppm to avoid $LiPF_6$ hydrolysis and HF formation [11]. Ambient preparation and handling of MeCN-based electrolytes often result in water levels in the tens to hundreds of ppm unless specific drying and inert-transfer procedures are applied [12]. Conventional analytical approaches, such as Karl Fischer titration or spectroscopic techniques (IR, Raman, NMR), provide accurate measurements of water content, but they are typically ex situ and require specialized instrumentation. Accordingly, the development of diagnostic electrochemical methods that can identify the early stages of electrolyte ageing and water-induced degradation in situ, while reducing the need for complex analytical instrumentation, remains an important objective.

Cyclic voltammetry (CV), although not quantitative, is a widely accessible technique to track changes associated with trace water and electrolyte ageing [13]. Variations in current response may therefore offer qualitative indicators of moisture-related degradation. Nevertheless, the sensitivity of the voltametric response depends strongly on the properties of the electrode surface. Studies have shown that platinum electrodes are particularly responsive to water traces and decomposition products in $LiPF_6$-based electrolytes [14,15], and that modifying their surface morphology can amplify such effects. Nanostructured platinum offers increased electroactive area, thereby improving sensitivity to faradaic processes associated with moisture or hydrolysis [16]. In addition, coatings such as Nafion provide selective ionic permeability and limit solvent access to the electrode surface, thereby modulating ion–solvent interactions [17].

Electrolyte ageing and water detection are closely interrelated phenomena. As moisture accumulates and hydrolysis proceeds, both the composition and the electrochemical stability of the solvent evolve, complicating the interpretation of voltametric signals and the identification of genuine water-related processes. In this work, we investigate the electrochemical behaviour of $Bu_4NPF_6$ and $LiPF_6$ electrolytes in MeCN under controlled water contamination. Lithium hexafluorophosphate ($LiPF_6$) was selected as the representative lithium salt because it remains a widely used electrolyte component in lithium-ion batteries, owing to its high ionic conductivity, compatibility with aprotic carbonate and nitrile solvents, and ability to form stable passivation layers on metal surfaces. Cyclic voltammetry was employed as a tool to monitor the evolution of redox features associated with electrolyte ageing. Platinum electrodes with distinct surface properties—flat, Nafion-coated, and nanostructured (nanoflower)—were compared to evaluate how electrode morphology influences sensitivity towards moisture and degradation products. The experiments were conducted in anhydrous acetonitrile using pre-dried salts and electrodes under an argon atmosphere to minimize external moisture, but the experimental design permitted conditions where small amounts of water could appear, enabling the early stages of solvent and salt degradation to be examined. The main objective was to identify characteristic voltametric signatures that can serve as early indicators of moisture-induced degradation, and to assess

the potential of nanostructured Pt as a sensitive platform for in situ electrolyte monitoring, bridging the gap between laboratory diagnostics and practical electrochemical detection.

## 2. Materials and Methods

The electrochemical experiments were performed in a two-compartment H-cell operated under a slight argon overpressure to minimize external water contamination. Cyclic voltammetry was performed in the 50 mL cell equipped with a 20 mm diameter and 170 µm thickness proton-exchange membrane (both supplied by Redoxme AB, Norrköping, Sweden). This technique was used to monitor possible electrochemical reactions and provided the basis for the data and figures presented in this article. A non-aqueous Ag/AgCl refillable electrode (6 mm diameter) was used as the reference electrode (RE). For simplicity, herein we will refer potentials as potential against the Ag/AgCl reference electrode. A 99.9% platinum electrode served as the counter electrode (CE), and different samples based on evaporated platinum substrates—bare, Nafion-coated, and nanostructured (nanoflower)—were employed as the working electrodes. These configurations were tested under comparable conditions to evaluate the influence of proton transport and surface morphology on lithium-ion electrolytes.

The electrolytes were prepared using tetrabutylammonium hexafluorophosphate ($Bu_4NPF_6 \geq 99.0\%$, Sigma-Aldrich, St. Louis, MS, USA) as the supporting salt and lithium hexafluorophosphate ($LiPF_6$, Sigma-Aldrich) as the lithium source. Anhydrous MeCN, 99.8%, Sigma-Aldrich) was used as solvent. Solutions of $Bu_4NPF_6$ were prepared at a concentration of 10 mM in 100 mL MeCN to minimize water adsorption by reducing the amount of salt handled. A 50 mM $LiPF_6$ stock solution was separately prepared in 50 mL of MeCN, which was later diluted to obtain 1, 5 and 10 mM working concentrations. All electrolyte preparations were carried out under dry argon to avoid moisture uptake. The salts were placed in separate three-necked flasks and gently heated using a heating mantle (Glassco 1500.EU.03, Ambala Cantt, India) at temperatures below 50 °C for less than 30 min to promote moisture removal. The central neck of each flask was connected to a vacuum pumping unit (Vacuubrand PC 3001 VARIOpro, McLeansville, NC, USA) to extract residual humidity before solvent addition. MeCN was then withdrawn from the storage bottle under an argon atmosphere using an argon-filled balloon and injected through one of the side necks while argon was allowed to flow by switching a three-way valve from vacuum to argon. Once the flasks were under argon, the solvent was added, and all openings were sealed with septa, wrapped with Parafilm, and stirred until the salts were fully dissolved.

The working electrodes were fabricated on silicon wafers coated with a 5 nm titanium adhesion layer followed by a 100 nm platinum layer, both deposited using an electron-beam evaporator. The wafers were diced into a grid pattern comprising 0.9 cm × 0.9 cm squares and 0.5 cm × 1.5 cm rectangles using a DISCO Dicing Saw DAD3350, Tokyo, Japan. Before using, the samples were sequentially cleaned with acetone and isopropanol, rinsed with deionized water, dried under an argon stream, and treated for 10 min in a UV–ozone cleaner (model 42 series, Jelight Inc., Irvine, CA, USA).

The synthesis of platinum nanoflowers (PtNFs) was mediated by a PS-b-P4VP diblock copolymer and carried out by pulsed electrodeposition using an SP300 computer-controlled potentiostat (BioLogic, Seyssinet-Pariset, France). The mechanism of copolymer-assisted nucleation and anisotropic growth under pulsed electrodeposition conditions, which is transferable to platinum systems, has been described previously in literature [18]. The electrodeposition was performed in an aqueous electrolyte containing a platinum precursor salt and 0.05 M KCl as supporting electrolyte. To promote the formation of Pt nanoflowers, the effects of metal precursor concentration and electrolyte pH were systematically investigated. After optimization, the platinum salt concentration was fixed at 500 mM, and

the pH of the electrolyte was adjusted and maintained at pH = 4 for 1 h without stirring prior to electrodeposition. These conditions favour controlled nucleation and hierarchical growth, leading to flower-like platinum morphologies. After deposition, the samples were thoroughly rinsed with distilled water and dried under a nitrogen flow.

A conventional three-electrode configuration was employed, consisting of a platinum grid as the counter electrode, a saturated calomel electrode (SCE) as the reference electrode, and the Pt chips coated with PS-b-P4VP as the working electrode. The pulsed electrodeposition was achieved by alternating the applied potential between −0.25 V (deposition step) and 0.00 V (rest step), with a pulse duration of 5 s per step over 120 cycles. The total electrodeposition time was fixed at 3 h. The formation of flower-like platinum nanostructures is governed by electrochemical parameters and by the presence of the PS-b-P4VP copolymer film, which acts as a coordinating and templating layer. After deposition, the samples were thoroughly rinsed with distilled water and dried under a nitrogen flow.

Top-view and 52° angle morphology of the PtNFs was examined by Focused Ion Beam Scanning Electron Microscopy (FIB-SEM) using a Helios NanoLab 650 system (FEI Company, Hillsboro, OR, USA) (Figure 1). Several magnifications (from ×70 to ×250,000) were used to evaluate morphology, homogeneity, and nanoflower size across different regions of the electrode.

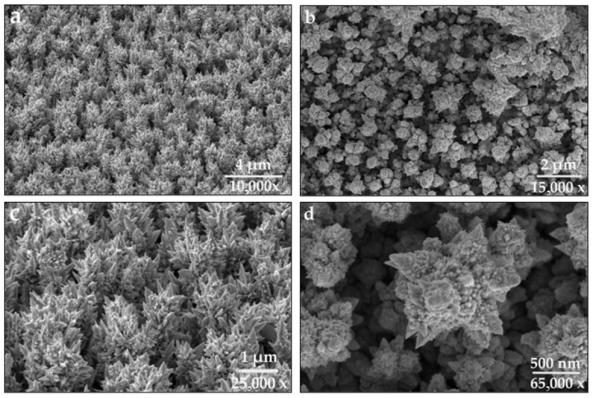



**Figure 1.** Focused Ion Beam–Scanning Electron Microscopy (FIB-SEM) images of the platinum nanoflower (PtNF) electrodes at different magnifications. Images (**a**,**c**) were acquired at 52° tilt and (**b**,**d**) at 0° tilt, showing nanostructure morphology.

Additional flat working electrodes were coated with a thin Nafion film. Thin Nafion coatings (~450 nm) were deposited by spin-coating (SPIN150i Tabletop, POLOS, New York, NY, USA) at 1500 rpm for 40 s after dispensing a droplet of Nafion solution onto the substrate. The coated electrodes were then cured at 150 °C for 45 min to ensure solvent removal and good adhesion. To standardize the electrode area and enable comparison between measurements, the active area of each electrode was determined using pictures of the submerged electrodes.

Cyclic voltammetry measurements were performed in the two-compartment H-cell placed inside a Faraday cage to minimize electrical noise and external interference. The cell was filled under an argon flow to prevent moisture ingress during electrolyte transfer. The background electrolyte, 10 mM $Bu_4NPF_6$ in MeCN, was first added to the CE compartment (6 mL) and then to the WE compartment (18–20 mL) until the sample and most of the proton-exchange membrane were covered. This base electrolyte was used to establish the initial electrochemical behaviour of the system by recording a CV at a scan rate of 10 mV $s^{-1}$ over a potential range of −2 V to +2 V. Subsequent CV experiments were performed at 20 mV $s^{-1}$ within the same potential window using a ModuLab XM ECS Electrochemical System (Solartron Analytical, Farnborough, UK). Argon was also flushed

in the cells between successive additions of 1, 5, and 10 mM $LiPF_6$ solutions to prevent moisture ingress. All measurements were performed at room temperature (22 ± 2 °C).

## 3. Results

### *3.1. Electrochemical Behaviour of the Baseline Electrolyte*

To establish the baseline electrochemical behaviour of the system in the absence of $Li^+$ ions or water ions, we performed several CV experiments exploring the maximum range that exhibited no peaks. Figure 2a shows the cyclic voltammograms obtained for the base electrolyte, 10 mM $Bu_4NPF_6$ in MeCN, recorded at a scan rate of 10 mV $s^{-1}$ using a 0.9 cm-wide platinum working electrode. The voltammograms appeared mostly flat across the potential window between −2 V and +2 V. No clear redox peaks were observed, suggesting that $Bu_4NPF_6$ in acetonitrile does not show significant electrochemical activity under these conditions.

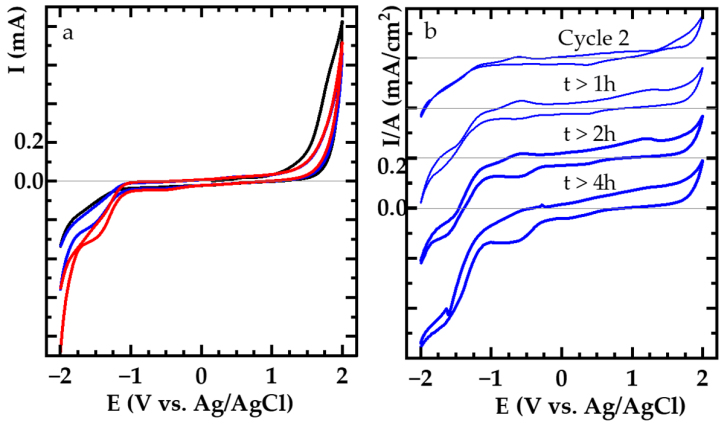



**Figure 2.** (**a**) Cyclic voltammograms recorded at 10 mV $s^{-1}$ on a flat platinum working electrode in the base electrolyte (10 mM $Bu_4NPF_6$ in MeCN). Curves in black, blue, and red correspond to the first, second, and third cycles, respectively. (**b**) Electrolyte ageing over 40 consecutive cycles recorded at 20 mV $s^{-1}$ on a flat platinum electrode.

After defining the initial electrochemical window of the supporting electrolyte, the same cell configuration was used to evaluate the time-dependent behaviour of the system and possible ageing effects. In this case, cyclic voltammetry was performed for 40 consecutive cycles using a 0.5 cm-wide flat platinum working electrode in 10 mM $Bu_4NPF_6$/MeCN at a scan rate of 20 mV $s^{-1}$. The scan rate increased to improve data sampling and accelerate the evaluation of possible ageing effects. Figure 2b compares early and late cycles recorded over four hours. Initially, the voltammogram displayed almost flat capacitive currents, characteristic of an electrochemically inert medium. However, the appearance of small, poorly defined features suggests that the presence of water cannot be excluded as the electrolyte ages with time. With continued cycling, a small cathodic peak appeared around −0.75 V, increasing gradually in intensity.

### *3.2. Effect of Water Addition*

After characterizing the electrolyte's behaviour over multiple cycles, controlled additions of water were performed to distinguish the specific effects of moisture from those arising during the natural evolution of the electrolyte. As shown in Figure 3, two sequential additions of 1 µL of water (≈50 ppm in the total electrolyte volume) were performed, each monitored over five cycles of CV. These additions led to a pronounced growth of the cathodic peak previously observed near −0.75 V, together with the appearance of a smaller one close to 0 V. We attribute the peak at 0 V to the reduction of hydrogen ions

dissolved in water. In aprotic media, the reduction of hydrogen dissolved in water at platinum produces hydrogen gas and hydroxide ions through the hydrogen evolution reaction (HER) [7] shown in Equation (1):

$$2H_2O + 2e^- \rightarrow H_2(g) + 2OH^- \quad (1)$$

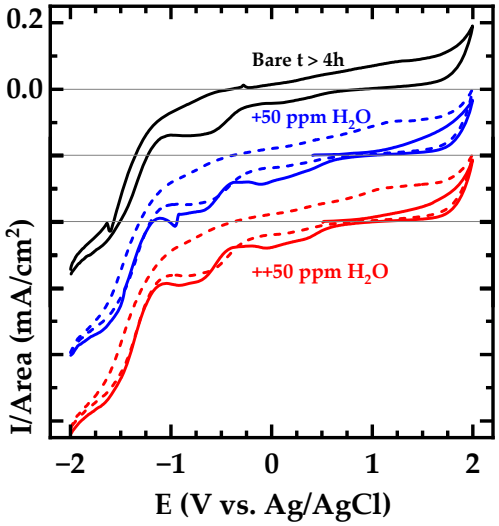



**Figure 3.** Cyclic voltammograms recorded at 20 mV $s^{-1}$ on flat platinum electrodes in 10 mM $Bu_4NPF_6$/MeCN after successive additions of 1 µL of water (≈50 ppm). The blue curves represent the voltammograms after the first addition, while the red curves correspond to the response following a second 1 µL addition. Dashed lines indicate the evolution during the subsequent cycle of each addition.

The hydrogen generated at the platinum surface nucleates as small bubbles that detach and escape into the argon atmosphere of the H-cell. This transient process disappears in subsequent cycles (red and blue dashed lines), as the water-based protonic species available for reduction are rapidly consumed and the produced hydrogen escapes from the system until new water is introduced.

To interpret the cathodic process observed between −0.75 and −1.0 V, we first considered the ionic and molecular species that may be present in the $Bu_4NPF_6$/MeCN electrolyte after water addition. The cyclic voltammograms recorded for the base electrolyte (Figure 2) confirmed that the tetrabutylammonium cation ($Bu_4N^+$) remains electrochemically inactive within the potential window employed. In contrast, the hexafluorophosphate anion $PF_6^-$ can undergo partial hydrolysis in the presence of trace moisture [4,9,19], forming $POF_3$, HF, and fluoride ions according to Equations (2) and (3):

$$PF_6^- + H_2O \rightarrow POF_3 + 2HF + F^- \quad (2)$$

$$HF \rightleftharpoons H^+ + F^- \quad (3)$$

The formation of HF, which remains in solution as a weak acid, introduces protonic species ($H^+$, $HF_2{}^-$, or $H_2O{\cdot}H^+$ complexes) capable of undergoing electrochemical reduction. These species are expected to influence the voltametric response, surface stability, and water-sensing behaviour of the system [14]. The HF and associated complexes produced in these reactions act as effective proton donors in the aprotic medium, where acetonitrile molecules cannot themselves participate in hydrogen bonding or proton transfer. Because HF is a weak acid in MeCN on the solvent $pK_a$ scale, bulk dissociation to free $H^+$ is limited; however, in the presence of $PF_6^-$ (weakly coordinating) and especially $F^-$ (strong hydrogen-bond acceptor), proton activity is governed by ion pairing and $HF_2{}^-$/(HF)_$xF^-$

formation rather than simple $HF \rightleftharpoons H^+ + F^-$ speciation. The protonic species adsorbed on the platinum surface are then electrochemically reduced through the hydrogen evolution pathway shown in Equation (4):

$$2H^*_{ads} + 2e^- \rightarrow H_2(g) \quad (4)$$

The cathodic process observed between −0.7 and −1.0 V vs. Ag/AgCl is therefore attributed not to the direct reduction of free ions in $H_2O$, but to similar protonic species that originate from HF and related complexes. This more negative feature likely corresponds to a slower, surface-controlled process involving HF-type species that form hydride-like intermediates ($H^-$ or $H_{ads}$). We attribute the occurrence of these steps at distinct potentials to the development of a thick interfacial double layer in the organic electrolyte, where the limited proton mobility compared with water leads to kinetically shifted reduction pathways. In acetonitrile, platinum electrodes exhibit hydrogen-related cathodic responses only in the presence of accessible proton donors, and the reduction potential strongly depends on the nature and mobility of the protonic species. While water-derived protons can be reduced at relatively mild cathodic potentials, weaker proton donors such as HF or $HF_2{}^-$—generated through $PF_6^-$ hydrolysis—require larger overpotentials due to solvent-specific solvation and interfacial kinetics. Previous studies of Pt voltammetry in MeCN have shown that trace water or acid-derived protonic species give rise to cathodic features shifted toward more negative potentials, consistent with the −0.7 to −1.0 V vs. Ag/AgCl process observed here [7,15].

### *3.3. Effect of $LiPF_6$*

We explored the possible effects of electrolyte composition in Li batteries, using additions of lithium hexafluorophosphate ($LiPF_6$). After the preparation of the electrolyte salt, a small amount of bright white precipitate was observed in the $LiPF_6$-based solutions. The amount of precipitate was minor relative to the initial salt quantity and was not removed, as the resulting solutions were used to evaluate qualitative electrochemical effects rather than absolute concentrations of lithium species.

Cyclic voltammetry was therefore conducted with the $LiPF_6$ nominal concentrations of 1, 5 and 10 mM in acetonitrile containing 10 mM $Bu_4NPF_6$ as the supporting electrolyte. As shown in Figure 4a, increasing the nominal concentration of $LiPF_6$ from 1 to 10 mM leads to a progressive enhancement of the cathodic peak located between −0.7 and −1.0 V vs. Ag/AgCl, while the anodic region remains almost unchanged.

The primary reactions expected upon $LiPF_6$ addition involve cleavage of the P–F bond to yield lithium fluoride (LiF), phosphorus oxyfluoride ($POF_3$), and hydrogen fluoride (HF), as represented in the Equations (5)–(7) below:

$$LiPF_6 + H_2O \rightarrow LiF\ (s) + POF_3 + 2HF \quad (5)$$

$$LiPF_6 \rightarrow LiF\ (s) + PF_5 \quad (6)$$

$$PF_5 + H_2O \rightarrow POF_3 + 2HF \quad (7)$$

These reactions generate solid LiF and HF-type species in solution. LiF may accumulate on the electrode or membrane surface, modifying interfacial conductivity or on the electrode surfaces, reducing the active surface area and consequently the peak currents. In practice, such effects would be expected to appear as reduced currents, broadened features, increased overpotentials, or progressive drift upon cycling. In our measurements, the voltametric response remained stable over repeated scans (no systematic peak shift or decay beyond experimental variability), suggesting that any LiF-related deposition is limited

under the conditions used. The HF formed can dissociate to produce protonic species ($H^+$, $HF_2^-$, or $H_2O{\cdot}H^+$ complexes) that contribute to the observed cathodic response. As shown in Figure 4a, increasing $LiPF_6$ concentration slightly shifts the cathodic peak toward less negative potentials, reflecting changes in the interfacial ion distribution rather than an intrinsic reduction of lithium ions.

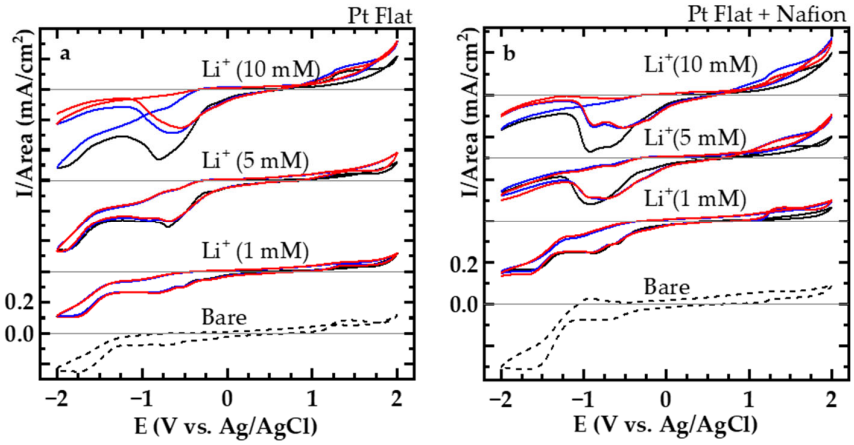



**Figure 4.** Influence of $LiPF_6$ concentration on the voltametric response. Cyclic voltammograms recorded at 20 mV $s^{-1}$ in 10 mM $Bu_4NPF_6$/MeCN after successive additions of $LiPF_6$. (**a**) Flat platinum working electrode. (**b**) Nafion-coated platinum working electrode. The color nomenclature follows the notation used previously: the dashed trace corresponds to the base electrolyte (second cycle), while the solid black, red, and blue curves represent the first, second, and third CV cycles, respectively, for the different lithium concentrations indicated in the graphs.

Although the formation of Li-containing intermediates cannot be completely ruled out, the deposition of metallic $Li^0$ is unlikely under these conditions, since MeCN lacks sufficient reductive stability to support lithium plating [20,21]. In non-aqueous electrolytes, lithium reduction typically occurs below −2.5 V vs. Ag/AgCl [22,23], beyond the potential range explored here. We attribute the increased intensity of the peaks in Figure 4a to the fact that additional $LiPF_6$ increases the concentration of $PF_6^-$, thereby increasing the conductivity of protonic species (The color coding in Figure 4 is consistent with the previous figures: the dashed line represents the base electrolyte (second cycle), and the solid black, red, and blue lines correspond to the first three CV cycles for the indicated lithium concentrations). Therefore, the enhancement of the −0.7 to −1.0 V feature with increasing $Li^+$ concentration is attributed to stronger $PF_6^-$ hydrolysis and higher availability of HF-derived proton donors rather than to lithium metal formation.

To further confirm that the cathodic response originates from protonic species formed during electrolyte ageing, cyclic voltammetry was performed using Nafion-coated platinum electrodes (Figure 4b). Nafion acts as a proton-conducting polymer that readily transports hydrogen ion species while limiting the motion of larger cations such as $Li^+$. This configuration therefore provides a convenient means of distinguishing ion-transport effects from intrinsic reduction processes. As shown in Figure 4b, the characteristic cathodic peaks between −0.7 and −1.0 V remain visible after coating with Nafion, although their intensity decrease and the potential shifts slightly toward more negative values.

Although Nafion can also transport $Li^+$ ions, we believe that under our experimental conditions the cathodic response is dominated by protonic species. Despite deliberate water addition, the electrolyte remains acetonitrile-based rather than fully hydrated, which limits $Li^+$ mobility within the Nafion phase. In addition, we observed identical cathodic features in Li-free control electrolytes upon water addition, indicating that $Li^+$ is not required for the appearance of the −0.7 to −1.0 V process. Moreover, while Nafion can

conduct $Li^+$, its selectivity toward protonic species remains the main contribution in predominantly aprotic environments. These considerations support a proton-mediated origin of the observed cathodic process rather than $Li^+$-controlled transport. We also observed an increase in the resistance to proton transport through the Nafion barrier (see Supplementary Figures S1 and S2).

This behaviour indicates that the process is mainly governed by protonic or HF-type species capable of diffusing through the Nafion barrier rather than by direct $Li^+$ reduction. The polymer layer thus modulates, but does not suppress, cathodic activity, supporting the interpretation that the observed signal arises from hydrogen-related reactions occurring within the electrolyte.

### *3.4. Influence of Electrode Nanostructuring*

The influence of the electrochemically active surface area on the system's sensitivity to electrolyte degradation was investigated using large surface area platinum nanoflower (PtNF) electrodes. These nanostructured surfaces exhibit a fractal structure responsible for a larger electrochemically active area compared with flat platinum, which can increase the density of adsorption sites and improve the detection of proton-coupled reactions. Controlled additions of water were subsequently introduced into the electrolyte to reproduce the early stages of solvent degradation and assess the material's ability to detect composition variations associated with the electrochemical response.

To further isolate the contribution of surface morphology from lithium-related effects, cyclic voltammetry experiments were performed comparing flat and nanostructured platinum electrodes of identical geometric area (0.5 cm width) in a Li-free 10 mM $Bu_4NPF_6$/MeCN electrolyte. Successive additions of water were carried out to examine how electrode roughness influences the cathodic response associated with protonic species. Figure 5 shows the comparison between the signals from the nanoflower electrodes and flat Pt. The full progression of water additions behaved similarly to the one observed in flat samples (see Figure S3 for the comparison with the full evolution). The PtNFs display a more pronounced increase in the cathodic currents associated with the protonic structures showing that the nanoflower platinum electrodes are more responsive to changes in the electrolyte. Considering the capacitive background of the CV, the integrated charge associated with the reduction peak was approximately five times higher for the PtNF electrodes than for the flat electrodes (see Table S1).

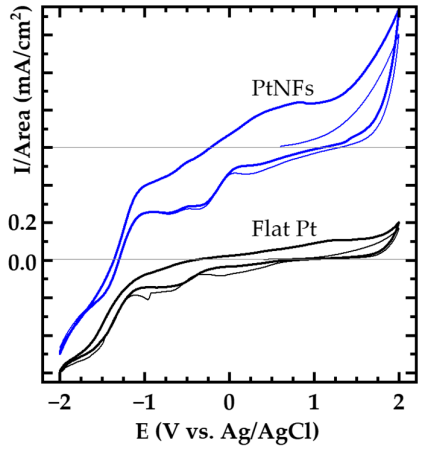



**Figure 5.** Cyclic voltammograms recorded at 20 mV $s^{-1}$ in 10 mM $Bu_4NPF_6$/MeCN after 1 µL of water (≈50 ppm) addition in the absence of $Li^+$. Comparison between flat platinum (black curves) and platinum nanoflower (blue curves). Working electrodes of equal geometric area (0.5 cm width). Fainter curves correspond to the first cycle recorded after each water addition.

## 4. Conclusions

This study presents cyclic voltametric experiments showing that trace levels of water in acetonitrile electrolytes induce characteristic cathodic features attributed to the formation and subsequent reduction of protonic species generated by $PF_6^-$ hydrolysis. The reproducibility of these signals across different electrode morphologies suggests their electrochemical origin and links them to solvent degradation processes. The evolution of the current response with cycling and water addition indicates that electrolyte ageing and water contamination are intrinsically coupled, as $PF_6^-$ decomposition continuously regenerates HF and related complexes, which are detected by the hydrogen-mediated redox reactions.

The introduction of $LiPF_6$ into the system shows an increase in this behaviour due to the higher availability of $PF_6^-$. The associated cathodic process remains visible at potentials between $-0.7$ and $-1.0$ V vs. Ag/AgCl, which is consistent with the reduction of adsorbed protonic species rather than with lithium deposition, which would be expected to occur at potentials more negative than $-2.5$ V in acetonitrile. The use of Nafion-coated electrodes further supports this interpretation; the cathodic peak persists despite the cationic selective barrier for $Li^+$, indicating that protonic or HF-type species are the dominant contributors to the observed reduction processes.

In addition to composition effects, electrode morphology plays a decisive role in determining sensitivity. Nanostructured platinum electrodes (Pt nanoflowers) exhibit higher current densities compared with flat platinum, evidencing a more efficient interaction with protonic species. Long-term stability tests of Pt nanoflowers have not yet been fully completed. However, analogous gold nanoflowers prepared under similar conditions exhibit good electrochemical and morphological stability, suggesting that Pt nanoflowers are likely to display comparable robustness; dedicated stability studies are currently underway.

As a result, the Pt nanoflower morphology provides a clearer and more stable electrochemical signature of water-induced degradation, highlighting its potential as a sensitive diagnostic platform for detecting moisture and ageing in non-aqueous electrolytes.

Our study supports the idea that cyclic voltammetry can identify electrochemical signatures associated with trace water contamination and electrolyte degradation in acetonitrile-based systems containing $PF_6^-$ salts. Future research should focus on establishing quantitative correlations between cathodic current and water concentration, optimizing sensitivity through electrode design, integration with device batteries and extending this methodology to other solvent–salt systems. Such developments would advance the implementation of electrochemical diagnostics as a practical alternative to conventional analytical techniques for real-time electrolyte monitoring.

**Supplementary Materials:** The following supporting information can be downloaded at: https://www.mdpi.com/article/10.3390/electrochem7010002/s1, Figure S1: Comparison of cyclic voltammograms recorded at 20 mV $s^{-1}$ in 10 mM $Bu_4NPF_6$/MeCN after successive additions of $H_2O$; Figure S2: Comparison of the reduction peak current (Ip) extracted from the voltammograms in Figure 2; Figure S3: Effect of water additions on the cyclic voltametric response of flat (a) and nanoflower (b) platinum working electrodes; Table S1: Integrated area.

**Author Contributions:** Conceptualization, E.A.-M., J.E.M. and C.P.G.; methodology E.A.-M., J.E.M., W.G., D.B. and C.P.G.; validation, E.A.-M., J.E.M., K.M. and C.P.G.; formal analysis, E.A.-M., J.E.M., D.B., D.F., K.M. and C.P.G.; investigation, E.A.-M., J.E.M., W.G., D.B., K.M. and C.P.G.; resources, D.F., K.M. and C.P.G.; data curation, E.A.-M. and C.P.G.; writing—original draft preparation, E.A.-M. and C.P.G.; writing—review and editing, all authors; visualization, all; supervision, C.P.G. and K.M.; project administration, K.M. and C.P.G.; funding acquisition, D.F., K.M. and C.P.G. All authors have read and agreed to the published version of the manuscript.

**Funding:** This research was funded by Fonds National De la Recherche Luxembourg and the M-ERA.NET consortia with the project INTER/MERA22/16525938/NanoTRAACES, NANOTRAACES, M-ERANET 9389.

**Institutional Review Board Statement:** Not applicable.

**Informed Consent Statement:** Not applicable.

**Data Availability Statement:** The original contributions presented in this study are included in the article/Supplementary Materials. Further inquiries can be directed at the corresponding author.

**Acknowledgments:** AI tools in this study were employed solely for language editing and bibliographic searches under human oversight. No scientific analyses, interpretations, or results in this work were generated by AI.

**Conflicts of Interest:** The authors declare no conflicts of interest.

## References

1. Liao, Y.; Zhang, H.; Peng, Y.; Hu, Y.; Liang, J.; Gong, Z.; Wei, Y.; Yang, Y. Electrolyte degradation during aging process of lithium-ion batteries: Mechanisms, characterization, and quantitative analysis. *Adv. Energy Mater.* **2024**, *14*, 2304295. [CrossRef]
2. Adebanjo, I.T.; Eko, J.; Agbeyegbe, A.G.; Yuk, S.F.; Cowart, S.V.; Nagelli, E.A.; Burpo, F.J.; Allen, J.L.; Tran, D.T.; Bhattarai, N.; et al. A comprehensive review of lithium-ion battery components degradation and operational considerations: A safety perspective. *Energy Adv.* **2025**, *4*, 820–877. [CrossRef]
3. Rufino Júnior, C.A.; Sanseverino, E.R.; Gallo, P.; Amaral, M.M.; Koch, D.; Kotak, Y.; Diel, S.; Walter, G.; Schweiger, H.G.; Zanin, H. Unraveling the degradation mechanisms of lithium-ion batteries. *Energies* **2024**, *17*, 3372. [CrossRef]
4. Xu, K. Nonaqueous Liquid Electrolytes for Lithium-Based Rechargeable Batteries. *Chem. Rev.* **2004**, *104*, 4303–4418. [CrossRef]
5. Aurbach, D. Review of selected electrode–solution interactions which determine the performance of Li and Li ion batteries. *J. Power Sources* **2000**, *89*, 206–218. [CrossRef]
6. Gireaud, L.; Grugeon, S.; Laruelle, S.; Yrieix, B.; Tarascon, J.M. Lithium metal stripping/plating mechanisms studies: A metallurgical approach. *Electrochem. Commun.* **2005**, *8*, 1639–1649. [CrossRef]
7. Ledezma-Yanez, I.; Díaz-Morales, O.; Figueiredo, M.C.; Koper, M.T.M. Hydrogen Oxidation and Hydrogen Evolution on a Platinum Electrode in Acetonitrile. *ChemElectroChem* **2015**, *2*, 1612–1622. [CrossRef]
8. Yeyoung, H.; Caleb, S.; Steven, P.H.; Glenn, T.; Bertrand, J.; Tremolet, D.V.; Jiang, C.S.; Schnabel, M.; Stradins, P.; Burrell, A.; et al. Effect of Water Concentration in LiPF6-Based Electrolytes on the Formation, Evolution, and Properties of the Solid Electrolyte Interphase on Si Anodes. *ACS Appl. Mater. Interfaces* **2020**, *12*, 49563–49573. [CrossRef]
9. Spotte-Smith, E.W.C.; Petrocelli, T.B.; Patel, H.D.; Blau, S.M.; Persson, K.A. Elementary Decomposition Mechanisms of Lithium Hexafluorophosphate in Battery Electrolytes and Interphases. *ACS Energy Lett.* **2023**, *8*, 347–355. [CrossRef]
10. El-Maiss, J.; Balakrishnan, D.; García, C.P. Universal control of proton concentration using an electrochemically generated acid compatible with miniaturization. *Nanoscale Adv.* **2022**, *4*, 3233–3242. [CrossRef]
11. Cao, X. Important factors for the reliable and reproducible preparation of non-aqueous electrolyte solutions for lithium batteries. *Commun. Mater.* **2023**, *4*, 10. [CrossRef]
12. Kosfeld, M.; Westphal, B.; Kwade, A. Moisture behavior of lithium-ion battery components along the production process. *J. Energy Storage* **2023**, *57*, 106174. [CrossRef]
13. Šimek, A.; Kazda, T.; Báňa, J.; Čech, O. Basic Method for Water Detection in $LiPF_6$ Based Electrolytes. *Monatshefte Für Chem.* **2024**, *155*, 313–317. [CrossRef]
14. Gámez, V.; Melle, G.; Climent, V.; Rosa, M.; Arán, -A.; Herrero, E.; Juan, M.F. New understanding of the voltammetry of platinum in non-adsorbing electrolytes. *Electrochim. Acta* **2025**, *512*, 145494. [CrossRef]
15. Suárez-Herrera, M.F.; Costa-Figueiredo, M.; Feliu, J.M. Voltammetry of Basal Plane Platinum Electrodes in Acetonitrile Electrolytes: Effect of the Presence of Water. *Langmuir* **2012**, *28*, 5286–5294. [CrossRef]
16. PDaubinger, P.; Kieninger, J.; Unmüssig, T.; Urban, G.A. Electrochemical characteristics of nanostructured platinum electrodes—A cyclic voltammetry study. *Phys. Chem. Chem. Phys.* **2014**, *16*, 8392–8399. [CrossRef]
17. Claire, A.F.; Zacher, P., III; Lehto, D.; Krahn, D.; Knoche Gupta, K.L. Electrochemical Characterization of Recast Nafion® Film-Modified Electrodes in Acetonitrile with Various Electrolytes. *Electrochem* **2024**, *5*, 574–584. [CrossRef]
18. Bauer, P.; Mougin, K.; Faye, D.; Buch, A.; Ponthiaux, P.; Vignal, V. Synthesis of 3D Dendritic Gold Nanostructures Assisted by a Templated Growth Process: Application to the Detection of Traces of Molecules. *Langmuir* **2020**, *36*, 11015–11027. [CrossRef]
19. Yang, H.; Zhuang, G.V.; Ross, P.N. Thermal stability of LiPF6 salt and Li-ion battery electrolytes containing $LiPF_6$. *J. Power Sources* **2006**, *161*, 573–579. [CrossRef]

20. Yamada, Y.; Furukawa, K.; Sodeyama, K.; Kikuchi, K.; Yaegashi, M.; Tateyama, Y.; Yamada, A. Unusual Stability of Acetonitrile-Based Superconcentrated Electrolytes for Fast-Charging Lithium-Ion Batteries. *J. Am. Chem. Soc.* **2014**, *136*, 5039–5046. [CrossRef]
21. Nilsson, V.; Younesi, R.; Brandell, D.; Edström, K.; Johansson, P. Critical evaluation of the stability of highly concentrated LiTFSI—Acetonitrile electrolytes vs. graphite, lithium metal and $LiFePO_4$ electrodes. *J. Power Sources* **2018**, *384*, 334–341. [CrossRef]
22. Liu, M.M.; Gao, D.; Zhang, H.Z.; Guo, Y.; Yu, X.; Deng, T. Electrodeposition of Lithium in Nonaqueous Solutions and Molten Salts. *Adv. Mater. Res.* **2013**, *791–793*, 216–219. [CrossRef]
23. Wang, L.; Wu, F.; Yao, Y.; Zhang, C. Lithium Metal Anode in Electrochemical Perspective. *ChemElectroChem* **2024**, *11*, 202400019. [CrossRef]

**Disclaimer/Publisher's Note:** The statements, opinions and data contained in all publications are solely those of the individual author(s) and contributor(s) and not of MDPI and/or the editor(s). MDPI and/or the editor(s) disclaim responsibility for any injury to people or property resulting from any ideas, methods, instructions or products referred to in the content.